FROM MAGMA-OCEAN CUMULATES TO MELT INCLUSIONS: CONSTRAINTS ON LUNAR MANTLE WATER A. Roy[1], A. Mallik[1], S. Schwinger[2], P. Moitra[1], Y. Guan[3], M. Bose[4], J. J. Barnes[5], A. G. Distel[4], R. L. Hervig[4] and M. A. Alyousef[1], [1]Department of Geosciences, University of Arizona, Tucson, AZ 85721, USA, [2]Institute of Planetary Research, German Aerospace Center, Berlin 12489, Germany, [3]Division of Geological and Planetary Sciences, California Institute of Technology, Pasadena, CA 91125, USA, [4]School of Earth & Space Exploration, Arizona State University, Tempe, AZ 85287, USA, [5]Lunar and Planetary Laboratory, University of Arizona, Tucson, AZ 85721, USA; arkadeeproy@arizona.edu

Introduction: Water in the Moon's interior exerts a primary control on the generation of mare basalts and pyroclastic deposits by lowering the mantle solidus and enhancing melt productivity. These volcanic products represent localized melting of the lunar mantle, and their occurrence depends on the distribution of water in the mantle. However, estimates of lunar mantle water contents span multiple orders of magnitude, from as little as ~64 ppb [1] to as much as ~260 ppm H_2O [2]. Such a wide range implies markedly different magmatic evolutions for the Moon, from limited, episodic volcanism to fluxes nearing those of terrestrial upper mantle contains ~50–200 ppm H_2O [3].

The wide range of inferred lunar mantle water contents reflects uncertainties in the initial water budget of the lunar magma ocean (MO) and its crystallization history. Additional controls include redox conditions, volatile loss during MO degassing, and the partitioning of water into nominally anhydrous minerals (NAMs) that constitute the mantle cumulates. Among these factors, the mineral–melt partition coefficients (or D) for H_2O in orthopyroxene and clinopyroxene are particularly important, as these phases dominate much of the lunar upper mantle [4]. Yet, existing constraints on D for NAMs are sparse for Fe-rich compositions and reducing conditions relevant to lunar MO crystallization. This study aims to experimentally constrain pyroxene D values for lunar MO conditions and link mantle cumulate H_2O contents to source regions of basalts via batch melting.

Methods: We conducted high-pressure, high-temperature experiments using a piston-cylinder apparatus to determine D between pyroxenes and melt under conditions analogous to late-stage lunar MO crystallization. Experiments were performed at 0.5–1.2 GPa and 1220–1440 °C in either graphite or iron capsules, which buffered the charges to redox conditions appropriate for the lunar interior. Water contents of 7 orthopyroxene and 7 clinopyroxene experiments with their coexisting melts were measured as $^{16}O^1H^-/^{30}Si^-$ using SIMS and nanoSIMS with Cs^+ primary beams. These data were combined with recently published plagioclase– [5,6], orthopyroxene–, and olivine–melt D [7] and used to quantify water abundance and distribution in the mantle stratigraphic column.

These experimentally derived partition coefficients were incorporated into coupled alphaMELTS and FXMOTR (from SPICES software package [8]) magma-ocean crystallization models using appropriate H_2–H_2O solubility relations [9,10]. Assuming no trapped interstitial liquid during MO crystallization, we calculated H_2O profiles for mantle cumulates using NAM–melt partition coefficients from the literature [5,6,11] together with the experimentally determined values from this study. These calculations define end-member mantle H_2O profiles (Fig. 1) that can reproduce H_2O contents in the ferroan anorthosite suite.

Although our experiments constrain how H_2O is distributed during MO crystallization, olivine-hosted melt inclusion (MI) H_2O contents are required to estimate mantle source water contents. We therefore used MI H_2O data from Apollo samples [12,13] together with batch melting calculations (F = 2–20%) to back-calculate mantle source H_2O abundances. Source depths were constrained using multiple-saturation-point (MSP) estimates for green, orange, red, and black glasses with comparable MI TiO_2 contents [12,14–16]. Bulk mantle H_2O distribution coefficients were then adjusted according to source mineralogies inferred from these MSP constraints.

Results: For compositions and conditions most relevant to lunar MO crystallization, we determine D for clinopyroxene = 0.0107–0.0172 and a maximum D for orthopyroxene = 0.028. The coexisting melt water contents span from 0.06 – 2.3 w.t.%. These values are systematically lower than many D estimates derived from terrestrial analogs (0.004–0.05 for clinopyroxene and 0.003–0.03 for orthopyroxene [11]), reflecting the combined effects of high Fe-Ti and low-Al

compositions, as well as reducing experimental conditions.

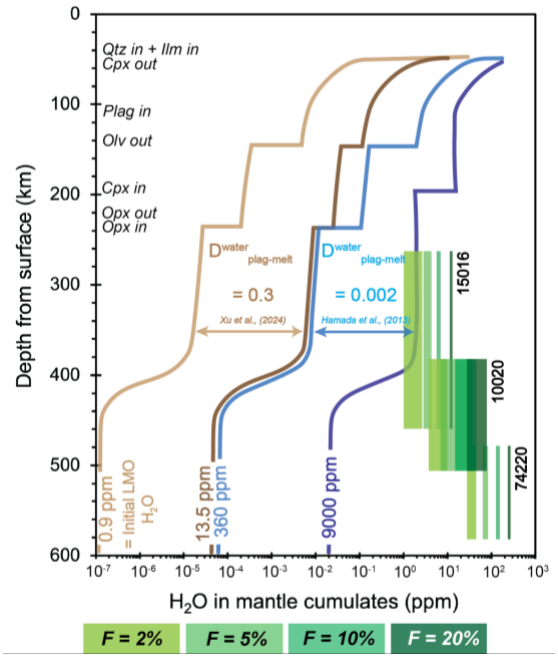


Figure 1. *Modeled H_2O contents of the lunar mantle cumulates versus depth for different assumed initial MO H_2O contents. Stepwise changes reflect major changes in phase assemblages during lunar MO crystallization. The gratings show estimated mantle source H_2O contents inferred from Apollo samples (74220, 10020, 15016) with F = 2 - 20%.*

In our models, initial MO H_2O contents were varied from 0.9–9000 ppm such that the resulting plagioclase H_2O concentrations reproduce the 2–6 ppm H_2O measured in ferroan anorthosite suite samples [17], the primary products of MO crystallization. Differences between model curves reflect variations in initial MO H_2O content, which primarily control the extent of degassing during early crystallization. In drier cases, degassing is negligible, whereas the wettest end-member undergoes substantial H_2O–H_2 loss.

When incorporated into MO crystallization models, these partition coefficients predict mantle cumulate water contents to increase in shallower conditions. Stepwise changes in modeled H_2O concentrations reflect major transitions in crystallizing mineralogy during MO solidification (Fig. 1).

Discussion: MI H_2O contents combined with batch melting calculations show that mantle water contents inferred from different Apollo samples are not mutually consistent, indicating localized mantle hydration [18]. Fig. 1 suggests that an initial MO water content of at least tens of ppm is required to reproduce the mantle source water contents inferred for samples 74220, 15016, and 10020. Accordingly, the plagioclase–melt partition coefficient of ~0.3 derived from 1-atm experiments on pure anorthite (An_{100}) [6] is likely too high to apply to An_{95} plagioclase crystallizing from the MO and forming the primary lunar crust.

The elevated MI H_2O contents of the high-Ti orange glass 74220 are inconsistent with cumulate mantle water abundances expected for a deep source region (480–580 km) and instead indicate hybridized source regions produced by mantle overturn [18,19]. In contrast, the olivine-normative basalt 15016 likely samples a more representative mantle source, requiring ~10^2–10^3 ppm H_2O with degrees of melting ≲5%, whereas the low-K ilmenite basalt 10020 reflects variable degrees of localized hydration. Within the parameter space explored, incorporation of trapped interstitial liquid during MO crystallization provides a viable mechanism to further increase mantle H_2O contents while maintaining lower initial MO water contents [20].

References: [1] McCubbin, F. M., et al. (2010). *PNAS, 107*, 11223-11228. [2] Saal, A. E., et al. (2008) *Nature, 454*, 192–195. [3] Hirschmann, M. M., (2006) *Annu. Rev. Earth Planet. Sci., 34,* 629-653. [4] Charlier B., et al. (2018) *GCA, 234,* 50–69. [5] Hamada, M., et al. (2013) *EPSL, 365*, 253–62. [6] Xu, Y., et al. (2024) *Chem. Geol, 661*, 122153. [7] Potts, N. J., et al. (2022) *GCA, 294,* 232-254. [8] Davenport, J. D., et al., *45th LPSC*, #1111. [9] Hirschmann, M. M., et al. (2012) *EPSL, 345–348,* 38–48. [10] Moore, G., et al. (1998) *AmMin, 83,* 36–42. [11] Mallik, A., et al (2022) *MaPS, 57,* 2143-2157. [12] Chen, Y., et al. (2015) *EPSL, 427,* 37-46. [13] Ni, H., et al. (2017) *EPSL, 478,* 214-224. [14] Elkins-Tanton, L. T., et al. (2003) *MaPS, 38*, 515-527. [15] Krawczynski, M. J., & Grove, T. L. (2012) *GCA, 79,* 1–19. [16] Wagner, T. P., & Grove, T. L. (1997) *GCA, 61,* 1315-1327. [17] Hui, H., et al. (2017) *EPSL, 473,* 14–23. [18] Robinson, K. L., & Taylor, G. J., (2014) *Nat. Geo., 7,* 401–408. [19]. Albarède, F., et al. (2014) *MaPS, 50,* 568-577. [20] McCubbin, F. M., et al. (2015). *Am. Min., 100*, 1668-1707.